Rapid Communications   Editors' Suggestion

Observation of strong higher-order lattice anharmonicity in Raman and infrared spectra

Xiaolong Yang [1,2,3,*] Tianli Feng,[1,*] Joon Sang Kang,[4] Yongjie Hu,[4] Ju Li,[5] and Xiulin Ruan[1,†]

[1]*School of Mechanical Engineering and the Birck Nanotechnology Center, Purdue University, West Lafayette, Indiana 47907-2088, USA*
[2]*Institute for Advanced Study, Shenzhen University, Shenzhen 518060, China*
[3]*Frontier Institute of Science and Technology, and State Key Laboratory for Mechanical Behavior of Materials,
Xi'an Jiaotong University, Xi'an 710049, China*
[4]*School of Engineering and Applied Science, University of California, Los Angeles (UCLA), Los Angeles, California 90095, USA*
[5]*Department of Nuclear Science and Engineering and Department of Materials Science and Engineering,
Massachusetts Institute of Technology, Cambridge, Massachusetts 02139, USA*

The fundamental theory of Raman and infrared (IR) linewidth has been well established as the third-order lattice anharmonicity (three-phonon scattering). In this work, we use both rigorous density functional calculations and Raman experiments to find, surprisingly, that the fourth-order anharmonicity universally plays a significant or even dominant role over the third-order anharmonicity at room temperature, and more so at elevated temperatures, for a wide range of materials including diamond, Si, Ge, GaAs, boron arsenide (BAs), cubic silicon carbide (3*C*-SiC), and α-quartz. This is enabled by the large four-phonon scattering phase space of zone-center optical phonons. Raman measurements on BAs were conducted, and their linewidth verifies our predictions. The predicted infrared optical properties through the Lorentz oscillator model, after including four-phonon scattering, show much better agreement with experimental measurements than those three-phonon-based predictions. Our work advances the fundamental understanding of Raman and IR response and will broadly impact spectroscopy techniques and radiative transport.

Phonon anharmonicity plays a key role in the linewidth of infrared and Raman spectra, which are basic material properties important for sensing, materials characterizations, radiative heat transfer including near-field radiation and radiative cooling, energy harvesting, and metamaterials [1,2]. It is also key to the dielectric function of polar dielectrics in the IR range, which can be effectively described by the Lorentz oscillator model [2]:

$$\epsilon(\omega) = \epsilon_\infty \left(1 + \sum_m \frac{\omega_{\mathrm{LO},m}^2 - \omega_{\mathrm{TO},m}^2}{\omega_{\mathrm{TO},m}^2 - \omega^2 - i\gamma_m\omega} \right), \qquad (1)$$

where ϵ_∞ is the dielectric constant at the high-frequency limit, ω is the photon frequency, ω_{TO} and ω_{LO} are frequencies of the zone-center TO (transverse optical) and LO (longitudinal optical) phonon modes, respectively, γ is the damping factor manifesting phonon anharmonicity and is equal to the zone-center optical phonon linewidth 2Γ, and m is the index of all the IR-active zone-center phonon modes. Phonon linewidth is generally difficult to measure at high temperatures due to thermal oxidation and self-radiation [3]. The available measured zone-center optical phonon linewidths have been explained in the framework of third-order phonon anharmonicity (three-phonon scattering) [4–9]. However, the predicted linewidths are considerably smaller than the experimental data, e.g.,

silicon at high temperature [4] and zinc-blende GaAs at room temperature [6], and the discrepancy was attributed to defect or impurity scattering. An attempt to include higher-order scattering through *ab initio* molecular dynamics [10] did not improve over the density-functional perturbation theory (DFPT) based on three-phonon scattering. A recent DFPT incorporating four-phonon scattering [11] considerably overestimated the zone-center phonon linewidth, which is difficult to interpret since the predicted intrinsic linewidth corresponds to a pristine crystal and should serve as a lower limit for experiments. Hence, the role of higher-order anharmonicity is still unclear.

In this work, we perform density functional theory calculations and Raman experiments to directly show that strong or even dominant higher-order phonon anharmonicity, not defects or impurities, is responsible for the larger-than-expected Raman and IR linewidth for a *wide* range of materials including diamond, Si, Ge, GaAs, BAs, 3*C*-SiC, and α-quartz at various temperatures. In many of the situations higher-order anharmonicity is negligible for acoustic phonons and thermal conductivity, but important for zone-center optical phonons and hence Raman and IR response. The phonon properties are predicted from the vibrational Hamiltonian, which can be Taylor expanded as $\hat{H} = \hat{H}_0 + \hat{H}_3 + \hat{H}_4 + \cdots$, where $\hat{H}_0$, $\hat{H}_3$, and $\hat{H}_4$ are the harmonic, cubic, and quartic terms, respectively. $\hat{H}_3$ induces the phonon linewidth by three-phonon scattering rates $\tau_{3,\lambda}^{-1}$ [12–14]. $\hat{H}_4$ induces four-phonon scattering rates $\tau_{4,\lambda}^{-1}$ [15–17]. We also include the effect of phonon-isotope scattering τ_{iso}^{-1} on the phonon linewidth [18].

*These authors contributed equally to this work.
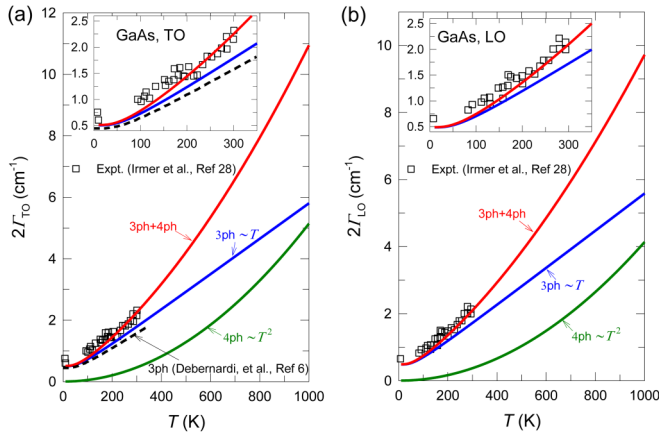†Corresponding author: ruan@purdue.edu.

FIG. 1. T dependence of the phonon linewidth, 2Γ, of the TO (a) and LO (b) modes in GaAs, with the insets for a better view below 300 K. The solid lines represent the results of the present calculation; the dashed lines denote the calculated result from Ref. [6]; the squares denote experimental data from Ref. [28].

Here the phonon linewidth is calculated under the single mode relaxation time approximation (SMRTA) by directly summing the normal and umklapp scattering rates. The phonon linewidth is associated with the decay rate of a phonon after its single mode excitation, where normal scattering contributes in a similar manner with the umklapp scattering. Therefore, SMRTA has been shown to generally work well for the prediction of phonon linewidth [4,19]. It can be noted that for thermal conductivity, on the other hand, umklapp scattering directly contributes to thermal resistance while normal scattering only indirectly contributes. Hence for predicting thermal conductivity, the SMRTA works for materials where umklapp scattering dominates, while the iterative approach should be used for materials with large normal scattering rates (such as diamond) [20]. Here the full width at half maximum 2Γ of a phonon mode is calculated as a Matthiessen sum of contributions from isotope scattering, three-phonon scattering, and four-phonon scattering rates:

$$2\Gamma = \gamma = \tau_{\text{iso}}^{-1} + \tau_{3,\lambda}^{-1} + \tau_{4,\lambda}^{-1}. \quad (2)$$

The formalism described above requires the second-, third-, and fourth-order interatomic force constants for calculating phonon frequencies and scattering rates, which were obtained from the Vienna *Ab initio* Simulation Package (VASP) [21] within the local density approximation, with the details given in Sec. A of the Supplemental Material [22]. Specifically, we use the four-phonon scattering formalism in Refs. [15–17], which has been validated by recent experiments on the high thermal conductivity of BAs [23–25] and extended to strongly anharmonic materials [26,27]. Our predicted phonon dispersions of all materials studied agree well with those measured in the literature as shown in Sec. B of the Supplemental Material [22] (see, also, Refs. [7–12] therein).

Taking GaAs as an example, we show the calculated T-dependent TO phonon linewidth in Fig. 1(a) with the inset for a better view below $T_{\text{room}} = 300$ K. Isotope scattering is included in all curves in this Rapid Communication unless noted otherwise. We find that the three-phonon scattering prediction

is considerably lower than the experimental data [28] even at T_{room}. With $\tau_{4,\lambda}^{-1}$ included, the prediction matches with experiment surprisingly well. Note that four-phonon scattering is negligible for thermal conductivity of GaAs at T_{room} [29,30]. Also, as T increases, our prediction of 2Γ including $\tau_{4,\lambda}^{-1}$ deviates significantly from that only involving $\tau_{3,\lambda}^{-1}$, as shown in Fig. 1(a). This indicates that four-phonon processes, which were neglected in the past, can actually remedy the discrepancies between previous calculations [6] and experiments. We also note that $\tau_{3,\lambda}^{-1}$ increases approximately linearly, whereas $\tau_{4,\lambda}^{-1}$ increases approximately quadratically with increasing T, consistent with Refs. [15,31]. Thus, $\tau_{4,\lambda}^{-1}$ becomes comparable to $\tau_{3,\lambda}^{-1}$ at mid to high temperatures. Similar significance of four-phonon scattering is also found for the LO branch as shown in Fig. 1(b).

Figure 2 shows the T-dependent optical phonon linewidths for diamond, Si, Ge, BAs, $3C$-SiC, and α- quartz, respectively. Similarly, only after including four-phonon scattering can we see good agreements with available experimental data from Refs. [32–38] and our own Raman spectra of BAs (see Sec. C of the Supplemental Material [22] for details). The difference between our three-phonon prediction and the previous calculation [4] in diamond is attributed to the isotope effect, which was not included in Ref. [4]. It should be noted that, unlike other materials, the experimental Raman spectra of BAs contain strong influence from isotope scattering [39]. We have subtracted such background contribution from both the experimental and the theoretical data, to leave only the T-dependent anharmonic linewidth for comparison. The agreement between prediction and experiment is excellent. It can be seen that in BAs the three-phonon processes have little contribution to the zone-center TO phonon linewidth due to lack of allowed scattering, and the four-phonon scattering totally dominates over three-phonon scattering in the entire T range. It should be noted that the T-induced phonon renormalization [40] may also affect phonon linewidths, which is not dealt with in the present work, but is non-negligible above the Debye temperature.

To gain a deeper insight into the microscopic mechanisms, we further analyze the contribution to $\tau_{4,\lambda}^{-1}$ from different scattering channels using BAs as an example. In Fig. 3(a), it can be seen that the dominant decay channels for zone-center optical phonons are the recombination process $\lambda_1 + \lambda_2 \rightarrow \lambda_3 + \lambda_4 + \mathbf{K}$, where $\mathbf{K}$ is a reciprocal lattice vector, which is zero for normal processes and nonzero for umklapp processes. These processes contribute more than 90% to $\tau_{4,\lambda}^{-1}$ of the zone-center optical phonon of BAs at 1000 K. Similar cases are also found in the other materials studied. The origin of such high $\tau_{4,\lambda}^{-1}$ of optical branches is illustrated in Fig. 3(b). The optical branches bunch together and allow the four modes $\lambda_1, \lambda_2, \lambda_3,$ and λ_4 to have similar energies. Alternatively, the summation of the energies of an optical phonon λ_1 and an acoustic phonon λ_2 can easily reach that of another optical phonon λ_3 and another acoustic phonon λ_4. Therefore, the energy conservation rule for the recombination process $\lambda_1 + \lambda_2 \rightarrow \lambda_3 + \lambda_4 + \mathbf{K}$ is easily satisfied. As a result, the optical branches often have large four-phonon scattering phase space. This is a key difference for phonon linewidth as compared to thermal transport, which is dominated by acoustic phonons
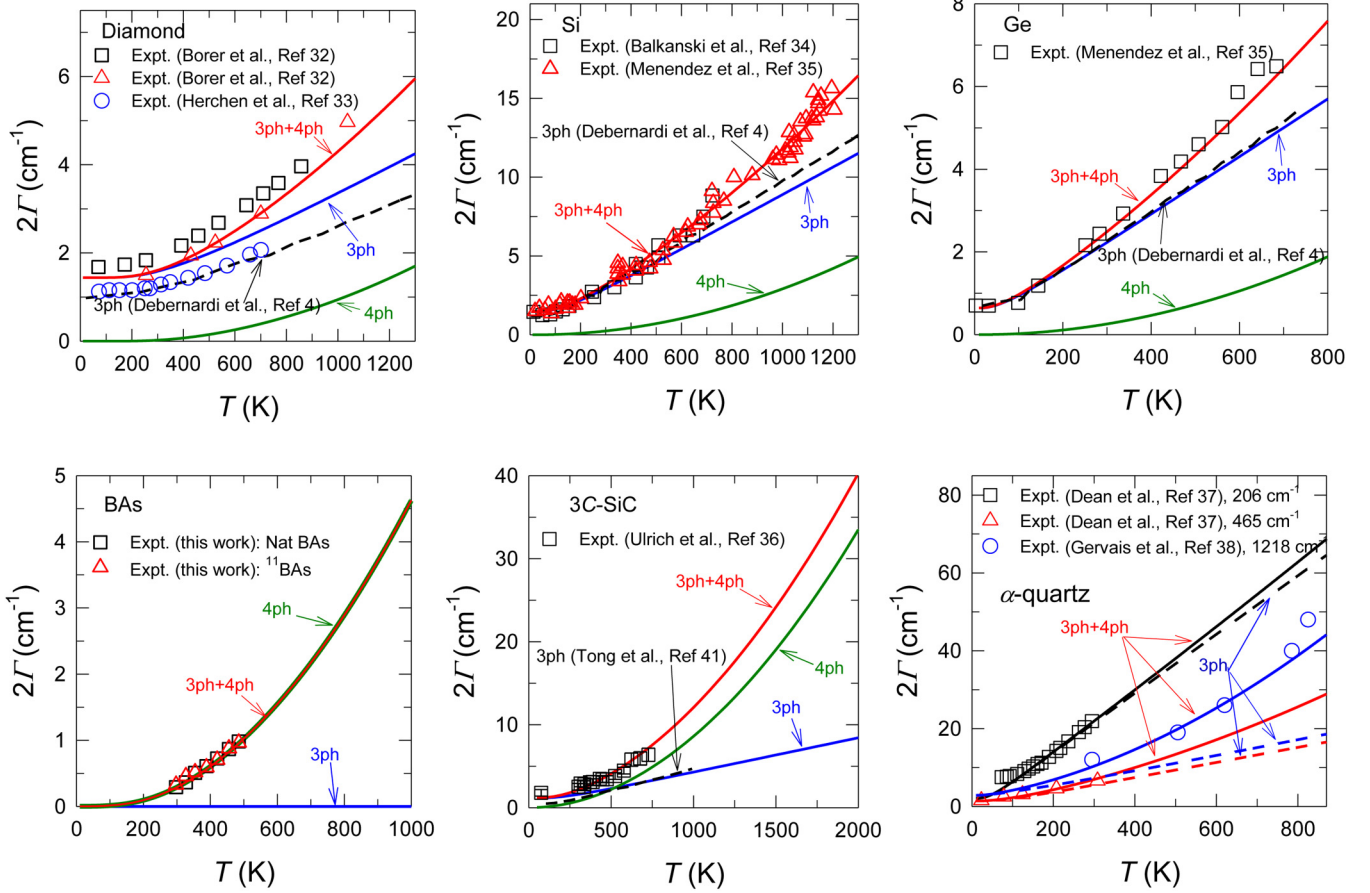
FIG. 2. Zone-center optical phonon linewidth in diamond, Si, Ge, BAs, 3C-SiC, and α-quartz as a function of T. For diamond, Si, and Ge, the solid curves represent the results of the present calculation, and the dashed curves denote the calculated results from Ref. [4]; all symbols denote experimental data from Refs. [32–35]. For BAs, the solid curves represent the results of our present calculations of the TO phonon linewidth; the black squares and red up triangles denote our Raman measurement for natural abundance and isotope pure BAs, respectively. For 3C-SiC, the solid curves represent our present prediction of the TO phonon linewidth; the black squares denote experimental data from Ref. [36]; the dashed curve represents the calculated result from Ref. [41]. For α-quartz, all curves represent our predicted phonon linewidth with (solid lines) and without (dashed lines) $\tau_{4,\lambda}^{-1}$ for phonon modes with frequencies of 206, 465, and 1218 cm^{-1}, and all symbols denote the experimental data from Refs. [37,38].

and strongly depends on the temperature, acoustic-optical gap, and anharmonicity of the materials. In other words, the significance of four-phonon scattering will be more broadly seen in zone-center optical phonon linewidth than in thermal conductivity.

With the predicted 2Γ combined with frequency values ω_{TO} and ω_{LO} listed in Supplemental Material Table S1 [22] (see, also, Refs. [12–16] therein), we address the importance of four-phonon scattering in dielectric function ϵ. The calculated ϵ with $\tau_{4,\lambda}^{-1}$ (red lines) for BAs, and the calculated ϵ with (red lines) and without (blue lines) $\tau_{4,\lambda}^{-1}$ for 3C-SiC and α-quartz at various T, are presented in Fig. 4(a). Here isotope scattering is excluded in BAs to make the anharmonic effects stand out. Remarkably, for isotopically pure BAs, the three-phonon scattering has almost no contribution and four-phonon scattering completely dominates the imaginary part of the dielectric function, ϵ_i. For 3C-SiC, with $\tau_{4,\lambda}^{-1}$ included the ϵ_i has a much broader peak, corresponding to a larger linewidth as highlighted by the solid arrow. We also find that when four-phonon scattering is added the peak value of ϵ_i decreases by 70% for 3C-SiC at 1000 K. For α-quartz, after introducing $\tau_{4,\lambda}^{-1}$, the peak values of the dielectric function at 785 K also have a significant reduction ranging from 20% to 50%
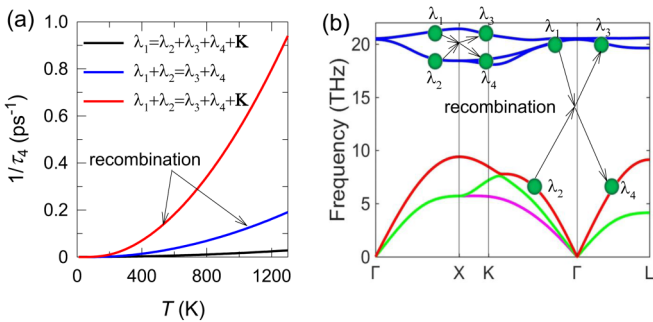

FIG. 3. (a) The contribution to $\tau_{4,\lambda}^{-1}$ of BAs from different scattering channels. (b) Phonon dispersion of BAs with schematic diagrams of four-phonon scattering processes dominated by recombination channels.
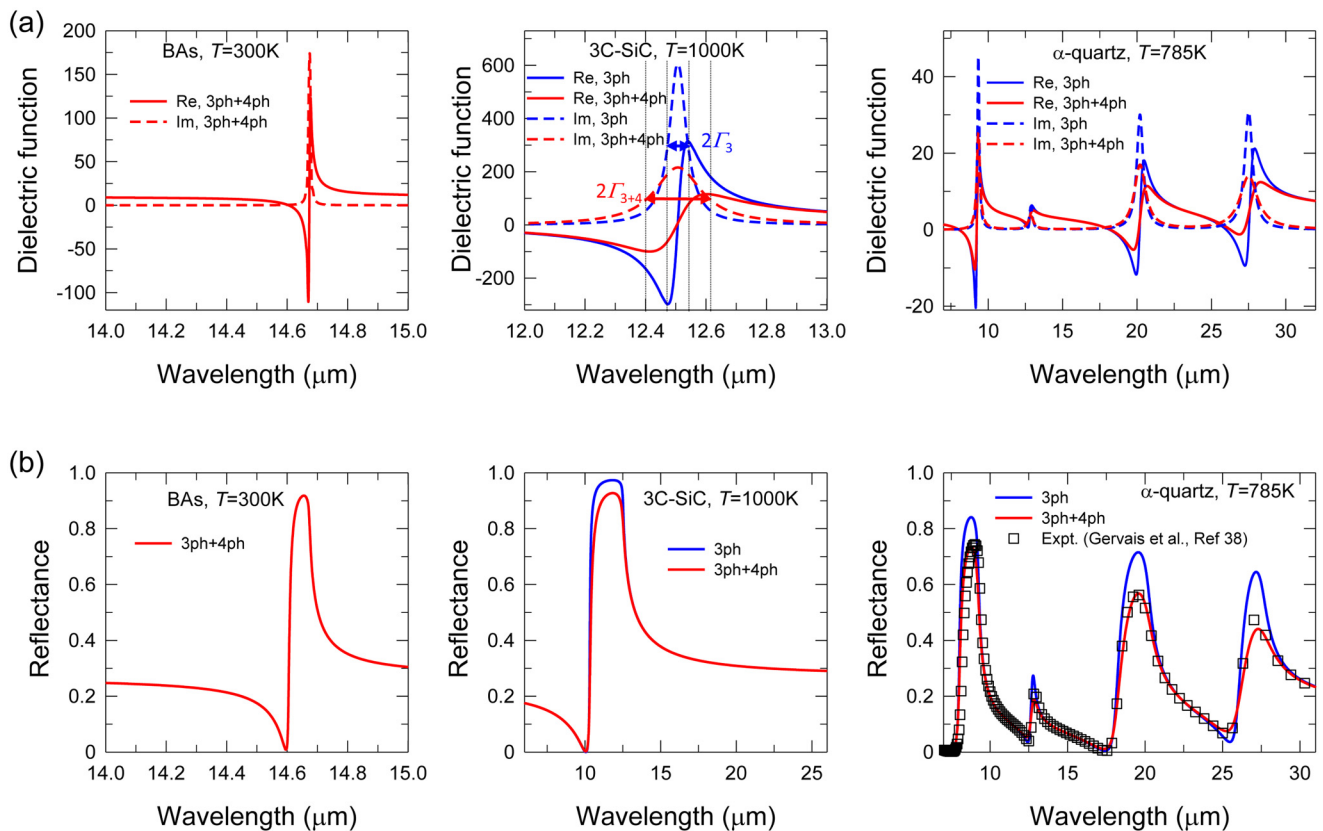
FIG. 4. (a) The calculated dielectric function of BAs, 3*C*-SiC, and α-quartz with (red lines) and without (blue lines) $\tau_{4,\lambda}^{-1}$ included. Solid lines represent the real part (Re) of dielectric function and dashed lines denote the imaginary part (Im) of dielectric function. (b) The calculated semi-infinite normal reflectance R for BAs at 300 K, 3*C*-SiC at 1000 K, and α-quartz at 785 K along with available experimental data [38] for comparison.

for different vibrational modes. These results suggest that previous works that considered three-phonon anharmonicity alone led to significant errors, and four-phonon scattering plays a decisive role in predicting high-temperature dielectric functions of IR-active materials.

With the complex dielectric function ϵ, the normal reflectance from a semi-infinite block R can be calculated as $R(\omega) = |(\sqrt{\epsilon(\omega)} - 1)/(\sqrt{\epsilon(\omega)} + 1)|^2$. In Fig. 4(b), we show our predicted reflectance R of BAs, 3*C*-SiC, and α-quartz at various T, and the latter is compared to the available experimental measurement in Ref. [38]. It is found that at T_{room} our four-phonon theory predicts the peak value of pure BAs reflectivity as much as ~ 0.9, which offers an important theoretical basis for experimental measurements. For 3*C*-SiC, with four-phonon scattering included, the peak of reflectivity in the range of 10–13 μm will reduce by 10%. For α-quartz, it can be observed that the predicted reflectance peak with $\tau_{4,\lambda}^{-1}$ decreases by 10%–30% as compared to that with only $\tau_{3,\lambda}^{-1}$, and matches exceptionally well with the existing IR data [38].

In conclusion, we have observed strong or even dominating fourth-order phonon anharmonicity in Raman and IR response by first-principles calculations and Raman measurements.

Our results on a series of technically important semiconductors demonstrate that the previously neglected four-phonon scattering generally dominates optical phonon linewidth at elevated and high temperatures, owing to the relatively large density of states and four-phonon scattering phase space of the zone-center optical phonons. With four-phonon scattering included, the infrared optical properties of α-quartz agree well with previous measurements. Our work thus reveals a crucial role of four-phonon scattering for zone-center optical phonons as in Raman and IR response.

[1] M. Born and K. Huang, *Dynamical Theory of Crystal Lattices*, International Series of Monographs on Physics (Clarendon, Oxford, 1988).

[2] Z. Zhang, *Nano/Microscale Heat Transfer* (McGraw-Hill, New York, 2007).

[3] H. Fujiwara, *Ellipsometry of Anisotropic Materials* (John Wiley & Sons, Ltd., New York, 2007).

[4] A. Debernardi, S. Baroni, and E. Molinari, Phys. Rev. Lett. **75**, 1819 (1995).

[5] G. Lang, K. Karch, M. Schmitt, P. Pavone, A. P. Mayer, R. K. Wehner, and D. Strauch, Phys. Rev. B **59**, 6182 (1999).

[6] A. Debernardi, Phys. Rev. B **57**, 12847 (1998).

[7] A. Debernardi, C. Ulrich, K. Syassen, and M. Cardona, Phys. Rev. B **59**, 6774 (1999).

[8] F. Bechstedt, P. Käckell, A. Zywietz, K. Karch, B. Adolph, K. Tenelsen, and J. Furthmüller, Phys. Status Solidi B **202**, 35 (1997).

[9] X. Tang and B. Fultz, Phys. Rev. B **84**, 054303 (2011).

[10] H. Bao, B. Qiu, Y. Zhang, and X. Ruan, J. Quant. Spectrosc. Radiat. Transfer **113**, 1683 (2012).

[11] G. Fugallo, B. Rousseau, and M. Lazzeri, Phys. Rev. B **98**, 184307 (2018).

[12] D. A. Broido, M. Malorny, G. Birner, N. Mingo, and D. A. Stewart, Appl. Phys. Lett. **91**, 231922 (2007).

[13] L. Lindsay, D. A. Broido, and N. Mingo, Phys. Rev. B **82**, 115427 (2010).

[14] L. Lindsay, D. A. Broido, and T. L. Reinecke, Phys. Rev. Lett. **109**, 095901 (2012).

[15] T. Feng and X. Ruan, Phys. Rev. B **93**, 045202 (2016).

[16] T. Feng, L. Lindsay, and X. Ruan, Phys. Rev. B **96**, 161201(R) (2017).

[17] T. Feng and X. Ruan, Phys. Rev. B **97**, 045202 (2018).

[18] A. Kundu, N. Mingo, D. A. Broido, and D. A. Stewart, Phys. Rev. B **84**, 125426 (2011).

[19] A. A. Maradudin and A. E. Fein, Phys. Rev. **128**, 2589 (1962).

[20] A. Ward, D. A. Broido, D. A. Stewart, and G. Deinzer, Phys. Rev. B **80**, 125203 (2009).

[21] G. Kresse and J. Furthmüller, Comput. Mater. Sci. **6**, 15 (1996).

[22] See Supplemental Material at http://link.aps.org/supplemental/10.1103/PhysRevB.101.161202 for the computational details, phonon dispersions for all of the materials examined in this work, and Raman spectroscopy characterization.

[23] J. S. Kang, M. Li, H. Wu, H. Nguyen, and Y. Hu, Science **361**, 575 (2018).

[24] S. Li, Q. Zheng, Y. Lv, X. Liu, X. Wang, P. Y. Huang, D. G. Cahill, and B. Lv, Science **361**, 579 (2018).

[25] F. Tian, B. Song, X. Chen, N. K. Ravichandran, Y. Lv, K. Chen, S. Sullivan, J. Kim, Y. Zhou, T.-H. Liu *et al.*, Science **361**, 582 (2018).

[26] Y. Xia, Appl. Phys. Lett. **113**, 073901 (2018).

[27] N. K. Ravichandran and D. Broido, Phys. Rev. B **98**, 085205 (2018).

[28] G. Irmer, M. Wenzel, and J. Monecke, Phys. Status Solidi B **195**, 85 (1996).

[29] T. Luo, J. Garg, J. Shiomi, K. Esfarjani, and G. Chen, Europhys. Lett. **101**, 16001 (2013).

[30] L. Lindsay, D. A. Broido, and T. L. Reinecke, Phys. Rev. B **87**, 165201 (2013).

[31] Y. P. Joshi, M. D. Tiwari, and G. S. Verma, Phys. Rev. B **1**, 642 (1970).

[32] W. Borer, S. Mitra, and K. Namjoshi, Solid State Commun. **9**, 1377 (1971).

[33] H. Herchen and M. A. Cappelli, Phys. Rev. B **43**, 11740 (1991).

[34] M. Balkanski, R. F. Wallis, and E. Haro, Phys. Rev. B **28**, 1928 (1983).

[35] J. Menendez and M. Cardona, Phys. Rev. B **29**, 2051 (1984).

[36] C. Ulrich, A. Debernardi, E. Anastassakis, K. Syassen, and M. Cardona, Phys. Status Solidi B **211**, 293 (1999).

[37] K. J. Dean, W. F. Sherman, and G. R. Wilkinson, Spectrochim. Acta, Part A **38**, 1105 (1982).

[38] F. Gervais and B. Piriou, Phys. Rev. B **11**, 3944 (1975).

[39] V. G. Hadjiev, M. N. Iliev, B. Lv, Z. F. Ren, and C. W. Chu, Phys. Rev. B **89**, 024308 (2014).

[40] O. Hellman, P. Steneteg, I. A. Abrikosov, and S. I. Simak, Phys. Rev. B **87**, 104111 (2013).

[41] Z. Tong, L. Liu, L. Li, and H. Bao, Phys. B (Amsterdam, Neth.) **537**, 194 (2018).